Time delay distribution in Bragg gratings

Fabio Ghiringhelli* and Mikhail N. Zervas[†]

Optoelectronics Research Centre, University of Southampton, Southampton SO17 1BJ, United Kingdom

A layer-by-layer analysis of the time delay of both reflected and transmitted light in one-dimensional photonic band-gap structures is developed and applied to uniform Bragg gratings. An effective Fabry-Pérot cavity is associated with every layer along the Bragg grating, multiple paths with a well defined layer traversal time are identified, and the average time is computed, introducing an appropriate weighting factor that accounts for interference between different paths. The analysis presented leads directly to a complex-valued time delay whose real part is shown to be equivalent to the classic phase time delay. Physical meaning is also given to the imaginary part. The local dwell time, interpreted as the average time spent by light in the layer independently of the final (transmitted or reflected) state, is proved analytically to be related to the energy density distribution when small index change gratings are considered. The time delay evolution is derived at different wavelengths and the nonuniform distribution along the grating is discussed. Nonintuitive features such as superluminal transmission time delay for propagation inside the band gap and negative reflection time delay close to transmission resonances are addressed. Finally, the effect of introducing a small perturbation in the structure is shown to be directly related to the local time delay and is proposed as a possible experimental measurement scheme for both its real and imaginary parts.

I. INTRODUCTION

The propagation of light in one-dimensional periodic or quasiperiodic media has been extensively studied, mainly in the context of the fundamental properties of photonic band gaps [1]. Multilayer mirrors, corrugated waveguides, and fiber Bragg gratings are among the most common implementations of such structures. These scattering structures are characterized by a high dispersion around the stop band edges and show significant variation in the group velocity as the wavelength is varied across the stop-band [2]. Compared to free space propagation, the group velocity v_g can be either increased for in-band-gap propagation or decreased close to transmission resonances, and significant time delay variations (where $\tau = L/v_g$) can be achieved with the introduction of nonuniform perturbations or defects [3].

However, only the time delay characteristic of the entire scattering region has been analyzed so far. Typically, a transfer matrix approach (based on coupled wave theory for fiber gratings [4,5] or on the actual layer parameters for multilayers [6]) is used to calculate the reflection and transmission coefficients and the time delay (phase time) is obtained by differentiation of the global phase retardation θ with respect to ω [3]. No knowledge of the local properties is gained. Questions such as "How is the time delay accumulated along the length?" and "Are there sections that are likely to affect the light propagation more than others?" are important for both physical and technological reasons. Only a layer-by-layer analysis of reflected and transmitted light behavior can give such insight.

The object of this paper is the derivation of analytical expressions for such local time delays $\tau_R(s)$ and $\tau_T(s)$ for reflected and transmitted light, respectively, their application to the simple but significant case of a uniform grating, and the analysis of locally perturbed structures as a possible experimental route to measuring them. It is worth noting that the derivation presented is structure independent and can be applied to any scattering medium, either uniform or nonuniform. The results obtained are likely to be helpful in energy storage characterization (important in active device design, i.e., distributed Bragg reflector and distributed feedback lasers [7]), design robustness analysis (a device is more sensitive to imperfections where the light actually dwells the most), and obviously in the design of devices with a particular dispersion (i.e., dispersion compensating fiber Bragg gratings [8]). Moreover, the approach derived can also contribute to the broad discussion about "traversal time under a potential barrier," which applies to both electromagnetic evanescent propagation and quantum particle tunneling (see [9] and references therein for an exhaustive review) because of the analogy between the Helmholtz and the time-independent Schrödinger equations [10].

In Ref. [11], a multilayer is considered and a Fabry-Pérot-like picture is proposed for layer-by-layer characterization. The structure is divided into two different sections preceding and following the currently investigated layer, and multiple reflections are experienced inside this effective cavity before either transmission or reflection takes place. The probability of each path is calculated through the reflectivity R and the transmissivity T, and since each possible path has a well defined associated transit time the average dwell time in the layer can be evaluated. In this analysis the propagating field is treated as a classical particle and the scattering probabilities are calculated by wave theory. But light is best described by a wave form and its field (probability amplitude) evolution. As pointed out elsewhere [12], the fictitious particle picture ("photon") can still be used, but only taking into account that it has to be associated with a probability ampli-

---

*Email address: fg1@orc.soton.ac.uk

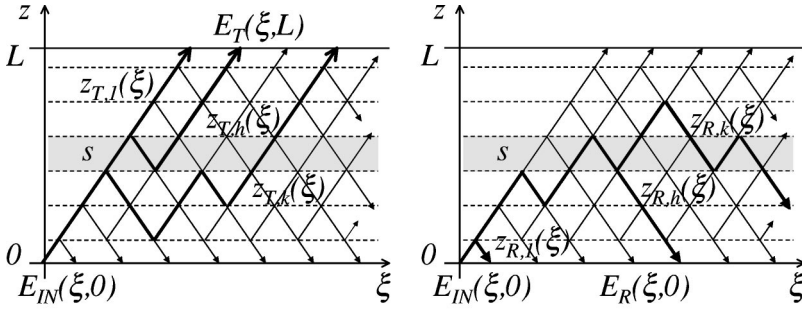[†]On sabbatical leave to Southampton Photonics Inc., Southampton SO16 7NS, U.K.

FIG. 1. Possible kth paths $z_{f,k}$ inside the grating due to multiple scattering, leading to either final transmission (left) or reflection (right).

tude $|\psi\rangle \rightarrow E$, i.e., a complex number with a phase that varies spatially. Moreover, "if a particle can reach a final state by two possible routes, the total amplitude for the process is the sum of the two routes considered separately" [13]. This means that, considering fields E (phase information retained) and not intensities I in the Fabry-Pérot-like picture, the infinite series of different paths leading to either transmission or reflection can be independently identified and their interference effects taken into account. Since a precise traversal time is associated with every single path, the average time delay of both transmitted and reflected photons can be evaluated in each grating section.

This approach was first introduced in Refs. [14,15]. It has recently been used by Lee *et al.* to analyze a single Fabry-Pérot cavity [16], and it was shown to be an application of Feynman paths in the spirit of Sokolovski and Connor [17]. A close relationship with the weak measurement theory for tunneling times developed by Steinberg [18] was also found.

In Sec. II, the local time delay will be defined and analytical expressions presented. The energy velocity will also be considered and the relationship with previously defined time delays discussed. The actual derivations are given in Appendix A, and the equivalence between the proposed approach and the phase time is analytically proved for uniform gratings in Appendix B. In Sec. III, the derived expressions will be applied to a uniform grating and the corresponding time delay distributions will be analyzed. In Sec. IV, the effects of grating perturbations are considered and shown to be related to the time delay obtained. This approach is proposed as a possible measurement method for local time delay.

II. DERIVATION OF TIME DELAY DISTRIBUTION

A. Approach to time delay computation

The mean traversal time of a certain section inside a scattering medium will be computed using the following definition [15]:

$$\tau_f(s) = \frac{\langle \psi_f | \hat{\tau}_f(s) | \psi_f \rangle}{\langle \psi_f | \psi_f \rangle} = \frac{\int \hat{\tau}_f(s) E_f^*(\xi) E_f(\xi) d\xi}{\int E_f^*(\xi) E_f(\xi) d\xi}. \quad (1)$$

$|\psi_f\rangle$ is the final state to be characterized, E_f is the associated electric field, s is the considered layer in the scatterer, and the integration is performed over the time ξ. In a grating of

length L, the final state is $|\psi_T\rangle \rightarrow E_f = E_T(\xi, L)$ for the transmission time delay and $|\psi_R\rangle \rightarrow E_f = E_R(\xi, 0)$ for the reflection time delay, where the fields are evaluated at time ξ and in position $z = L$ or 0, respectively. The traversal time operator through s can be defined once the actual kth path $z_{f,k} = z_{f,k}(\xi)$ to reach the considered final state $|\psi_f\rangle$ at time ξ is known:

$$\hat{\tau}_{f,k}(s) = \int \Theta_s[z_{f,k}(\xi)] d\xi, \quad \Theta_s[z_{f,k}] = \begin{cases} 1 & \text{if } z_{f,k} \in s, \\ 0 & \text{if } z_{f,k} \notin s, \end{cases} \quad (2)$$

where Θ_s selects only the portion of the path spent inside the investigated layer s. Given a possible path $z_{f,k}(\xi)$, the related time delay is well defined and unique.

As Fig. 1 shows, in a grating the distributed scattering produces a continuum of possible different trajectories $\{z_{f,1}, z_{f,2}, \ldots, z_{f,k}, \ldots\}$ for each final state $|\psi_f\rangle$ and therefore

$$\hat{\tau}_f(s) = \int_k \hat{\tau}_{f,k}(s) \delta_{f,k} dk, \quad (3)$$

where $\delta_{f,k}$ means that the time delay operator $\hat{\tau}_{f,k}(s)$ has to be associated only with the contribution $|\psi_{f,k}(s)\rangle$ of the path $z_{f,k}$ to the final state $|\psi_f\rangle$:

$$\hat{\tau}_f(s) |\psi_f(s)\rangle = \int_k \hat{\tau}_{f,k}(s) \delta_{f,k} |\psi_f(s)\rangle dk$$

$$= \int_k \tau_{f,k}(s) |\psi_{f,k}(s)\rangle dk \quad (4)$$

with time delay eigenvalue $\tau_{f,k}(s)$. Using Eq. (4), Eq. (1) may be written in a more concise way:

$$\tau_f(s) = \int_k \tau_{f,k}(s) \frac{\langle \psi_f | \psi_{f,k}(s) \rangle}{\langle \psi_f | \psi_f \rangle} dk$$

$$= \int_k \tau_{f,k}(s) \frac{\int E_f^*(\xi) E_{f,k}(\xi) d\xi}{\int E_f^*(\xi) E_f(\xi) d\xi} dk$$

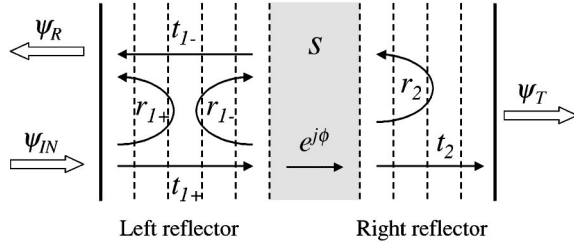$$= \int_k \tau_{f,k}(s) P_{f,k} dk, \quad (5)$$

FIG. 2. The selected layer s (shaded area) divides the structure into three different regions. The reflectors on either side are fully characterized by reflection and transmission coefficients, while the layer s is characterized by its phase delay ϕ (free propagation approximation).
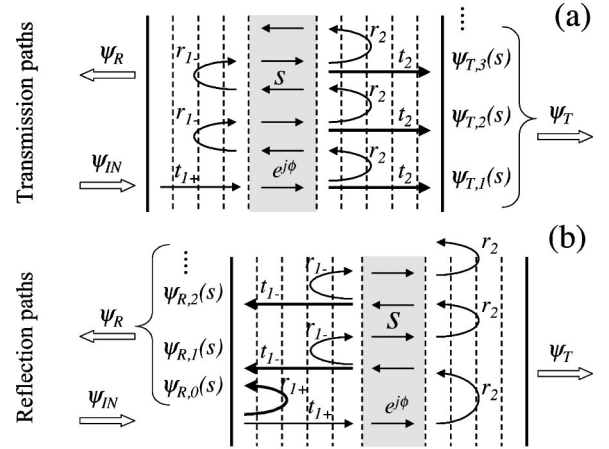

FIG. 3. Possible paths leading to photon transmission (a) and reflection (b) according to multiple scattering. Note that in reflection $|\psi_{R,0}(s)\rangle$ does not reach the layer s (shaded area).

where $\langle\psi_f|\psi_{f,k}(s)\rangle$ is the projection of each field component $|\psi_{f,k}(s)\rangle$ onto the global field $|\psi_f(s)\rangle$. This means that each $\tau_{f,k}(s)$ has to be weighted by how much the corresponding path contributes to the global field. In Eq. (5), a generally complex probability $P_{f,k}$ can be formally identified, since it can be directly shown that $\Sigma_k P_{f,k}=1$. Indeed, the $\hat{\tau}_f(s)$ operator so defined is non-Hermitian due to the nonorthogonality of the final state components $|\psi_{f,k}(s)\rangle$. Therefore the occurrence of complex probabilities and complex eigenvalues $\tau_f(s)$ is expected [18]. The related physical picture corresponds to the interference between different paths at either side of the structure when coherent fields are considered [15]. Introducing a complex-valued time delay may seem odd and nonphysical, but in Sec. III it will be shown that $\text{Re}\{\tau_f(s)\}$ is associated with well established time delay definitions. In Sec. IV a physical meaning will also be given to $\text{Im}\{\tau_f(s)\}$ [16].

The approach described leads to the computation of the "center of mass" arrival time if applied to pulse propagation and to the whole grating length [14]. The main advantage of the proposed formalism is the possibility of analyzing the time delay characteristics of the structure layer by layer, provided that all the possible paths $|\psi_{\text{in}}\rangle\rightarrow|\psi_f\rangle$ and the corresponding contributions $|\psi_{f,k}\rangle\rightarrow E_{f,k}(\xi)$ are identified.

Equation (5) looks different from expression (7) reported in Ref. [15], where the same time delay definition is applied to propagation through a dielectric slab, i.e., a Fabry-Pérot cavity. However, it has been analytically verified that the same final expressions are obtained by applying Eq. (5) to the same scattering structure, but with less involved computations and with a clearer physical understanding. For this reason the Eq. (5) formalism will be used in the rest of the study.

B. Fields and time delay computation

We start by considering an input field $|\psi_{\text{in}}\rangle$ entering the structure as shown in Fig. 2 and a generic layer s inside it. The considered layer is treated in the following derivation as a free space propagation region, i.e., only straight trajectories $z_{f,k}(\xi)$ are possible inside s. This approximation is valid as long as the layer length $\Delta L(s)$ is small compared to the inverse of the coupling constant κ, which means that the probability of a scattering event inside it is negligible.

With respect to s, the grating can be seen as a Fabry-Pérot cavity in which the left (labeled 1) and right (labeled 2) reflectors are fully characterized by their reflection and transmission coefficients r and t shown in Fig. 2. The complex coefficients r_{1+} and t_{1+} refer to forward propagating paths in the left reflector (left to right), and r_{1-} and t_{1-} to backward propagating paths (right to left). In a reciprocal medium, the general relation $t_{1+}=t_{1-}$ holds [19]. Note that the transmission and reflection coefficients are dispersive and different for every considered layer s, but the notation $t=t(\omega,s)$, $r=r(\omega,s)$ will be used later on for the sake of simplicity. In the following analysis a monochromatic excitation $|\psi_{\text{in}}\rangle\rightarrow E_{\text{in}}=e^{j(\beta z-\omega_0\xi)}$ will be considered, i.e., steady state conditions will be assumed, and only the lossless case, where the relation $R+T=|r|^2+|t|^2=1$ holds, will be addressed. It is also useful to introduce the round-trip reflection coefficient ρ of the effective Fabry-Pérot cavity associated with layer s:

$$\rho=r_{1-}r_2 e^{j2\phi}, \tag{6}$$

where $\phi=\beta\Delta L(s)=\omega_0\Delta\tau_0(s)$ is the phase delay for a single pass through the layer, with layer length $\Delta L(s)$ and layer time delay $\Delta\tau_0(s)=\Delta L(s)/v_{\text{eff}}=n_{\text{eff}}\Delta L(s)/c$.

As shown in Figs. 3(a) and 3(b), a discrete set of possible paths $\{z_{f,0},z_{f,1},\ldots,z_{f,k},\ldots\}$ with a well defined time $\tau_{f,k}(s)$ spent inside the layer s can be associated with both the transmitted $|\psi_T\rangle$ and reflected $|\psi_R\rangle$ final states. Knowing r and t expressions for the given structure (for instance, through a transfer matrix approach [5,6,19]), the final state can be computed and expressed through its $|\psi_{f,k}(s)\rangle$ components. In transmission,

$$|\psi_T\rangle=|\psi_{\text{in}}\rangle t_{1+}t_2 e^{j\phi}\sum_{k=0}^{\infty}\rho^k \tag{7a}$$

$$=|\psi_{\text{in}}\rangle\frac{t_1+t_2 e^{j\phi}}{1-\rho}=|\psi_{\text{in}}\rangle t_{\text{gr}}, \tag{7b}$$

where t_{gr} is the transmission coefficient of the whole grating. With a similar analysis in reflection,

$$|\psi_R\rangle = |\psi_{in}\rangle \left[r_{1+} + t_{1+}r_2t_{1-}e^{j2\phi}\sum_{k=0}^{\infty}\rho^k \right] \qquad (8a)$$

$$= |\psi_{in}\rangle \frac{r_{1+}+r_2(t_{1+}/t_{1+}^*)e^{j2\phi}}{1-\rho} = |\psi_{in}\rangle r_{gr}, \qquad (8b)$$

where r_{gr} is the total grating reflection coefficient. The expressions obtained with this approach are consistent with transfer matrix results, and each path component $|\psi_{f,k}(s)\rangle$ is clearly shown in Eqs. (7a) and (8b). This identification allows us to perform a weighted average over all possible interfering paths and to calculate the layer time delay according to Eq. (5).

The detailed derivation of both transmitted and reflected time delays is presented in Appendix A. The time delay $\tau_T(s)$ accumulated in layer s by transmitted light is found to be

$$\tau_T(s) = \frac{\langle\psi_T|\hat{\tau}_T(s)|\psi_T\rangle}{\langle\psi_T|\psi_T\rangle} = \Delta\tau_0(s)\frac{1+\rho}{1-\rho}. \qquad (9)$$

$\tau_T(s)$ is evaluated by taking into account that each field component $|\psi_{T,k}(s)\rangle$ in Fig. 3(a) experiences $(2k-1)$ passes in the layer due to multiple scattering in the grating before being transmitted. An important feature of Eq. (9) is that the real part of the transmission time delay is always positive in every layer, as shown by Eq. (A3a). Equation (9) is a generalization of Eq. (10) in Ref. [16].

Starting from Eq. (8b), the reflection time delay $\tau_R(s)$ becomes

$$\tau_R(s) = \frac{\langle\psi_R|\hat{\tau}_R(s)|\psi_R\rangle}{\langle\psi_R|\psi_R\rangle}$$

$$= 2\Delta\tau_0(s)\frac{T_1}{1-\rho}\frac{\rho}{\rho-R_1}, \qquad (10)$$

where T_1 and R_1 are the left mirror transmissivity and reflectivity, respectively. With reference to Fig. 3(b), it is worth noting that the time spent in layer s by $|\psi_{R,0}(s)\rangle$ is $\tau_{R,0}(s)$ $=0$ since these photons are reflected before reaching the layer, while for all the other field components $\tau_{R,k}(s)$ $=2k\Delta\tau_0(s)$. The real part of $\tau_R(s)$ can be shown to be negative for certain wavelengths and in certain grating positions. A possible justification of this nonintuitive result will be given in Sec. III, describing uniform grating calculations.

Using Eqs. (9) and (10), the overall time $\tau_{tot}(s)$ spent in layer s by a photon can be derived, independently of its transmitted or reflected final state. Since the final states are different, the two fields do not interfere and $\tau_{tot}(s)$ is given by the average value weighted by each final state probability (given by the transmissivity T_{gr} and reflectivity R_{gr} of the whole grating) [13,20]:

$$\tau_{tot}(s) = \tau_T(s)T_{gr} + \tau_R(s)R_{gr}$$

$$= \Delta\tau_0(s)T_{gr}\frac{1+R_2}{1-R_2}, \qquad (11)$$

where R_2 is the right mirror reflectivity. It is important to note that the total time delay so computed is always real and positive, despite the fact that the two independent components are complex. The physical explanation of this distinctive feature will be given in Sec. II C, where $\tau_{tot}(s)$ will be shown to be related to the energy density distribution inside the scatterer. Equation (11) corresponds to the result presented in Ref. [11].

Since $\tau_{tot}(s)$ is real, Eq. (11) can be expanded as

$$\tau_{tot}(s) = \text{Re}\{\tau_T\}T_{gr} + \text{Re}\{\tau_R\}R_{gr}, \qquad (12a)$$

$$0 = \text{Im}\{\tau_T\}T_{gr} + \text{Im}\{\tau_R\}R_{gr}, \qquad (12b)$$

where the corresponding expressions for the real and imaginary parts of the time delay are given by Eqs. (A3) and (A7). Equation (12b) is a direct consequence of energy conservation, as will be shown in Sec. IV.

From the previously calculated expressions, it is possible to characterize the time delay of the entire grating by simply summing up all the individual layer contributions:

$$\tau_f = \sum_s \tau_f(s) \qquad (13)$$

where f stands for T, R, or "tot." The equivalence of the real part of Eq. (13) for reflected and transmitted light with the classic phase time delay [3] cannot be proved by a general analytic derivation. An analytic proof can be obtained only in the uniform grating case, and it is derived in Appendix B.

C. Energy distribution and dwell time

The electromagnetic energy density distribution U inside the scatterer and the Poynting vector $\vec{S}$ (related to energy flux) can be easily derived knowing the field distribution in the various sections [21]:

$$U = \tfrac{1}{4}\epsilon_0 n_{eff}^2|\vec{E}|^2 + \tfrac{1}{4}\mu_0|\vec{H}|^2, \qquad (14)$$

$$\vec{S} = \tfrac{1}{2}\text{Re}\{\vec{E}\times\vec{H}^*\}, \qquad (15)$$

where ϵ_0 and μ_0 are the vacuum permittivity and permeability and n_{eff} is the effective refractive index.

Considering purely transverse fields, the electric field E $= E_0 e^{j(\beta z - \omega_0\xi)}$ is scalar and can be calculated in every position inside the structure with the multiple scattering picture described above, which is equivalent to the transfer matrix method. Considering the fields at the end of each layer, the forward and backward propagating fields E_+ and E_- in layer s are

$$E_+(s) = E_{in}\frac{t_{1+}e^{j\phi}}{1-\rho}, \qquad (16a)$$

$$E_-(s) = E_+(s)r_2, \qquad (16b)$$

and, as shown by normal mode analysis [22,23], the total electric and magnetic fields are expressed in term of these components as follows:

$$E_{\text{tot}}(s) = E_+(s) + E_-(s), \qquad (17a)$$

$$H_{\text{tot}}(s) = \frac{\beta}{\omega_0 \mu_0}[E_+(s) - E_-(s)]. \qquad (17b)$$

According to Eqs. (14), (16), and (17), the energy density distribution along the grating is given by

$$U(s) = \frac{1}{2}\epsilon_0 n_{\text{eff}}^2 |E_{\text{in}}|^2 T_{\text{gr}}\frac{1+R_2}{1-R_2}. \qquad (18)$$

In Eq. (18), the longitudinal dependence of the effective refractive index inside the considered layer s has not been explicitly taken into account and the average value n_{eff} is considered. This approximation is valid only for structures in which the refractive index contrast is small, such as fiber Bragg gratings. Typically, these gratings are centimeters long and the refractive index change is $\delta n \approx 10^{-4}$. Instead, in multilayer structures which are only micrometers long and have $\delta n > 10^{-1}$, the local expression for $n_{\text{eff}} = n_{\text{eff}}(z)$ has to be used and slightly different results are obtained [24]. In this case, the analytical equivalence presented in the following [see Eq. (20)] is not strictly valid.

Using Eqs. (15), (16), and (17), it is possible to evaluate the net Poynting vector flux $S(s)$ inside the grating along the propagation direction z:

$$S(s) = \frac{\beta}{2\omega_0 \mu_0}|E_{\text{in}}|^2 T_{\text{gr}} = S_{\text{in}}T_{\text{gr}}, \qquad (19)$$

where $S_{\text{in}} = \frac{1}{2}n_{\text{eff}}\sqrt{\epsilon_0/\mu_0}|E_{\text{in}}|^2$ is the flux of the incident transverse wave. The Poynting flux is found to be constant along the grating and related to the incoming flux S_{in} through the grating transmissivity T_{gr}, as expected because of energy conservation in passive, lossless media under steady state conditions.

Using Eqs. (11) and (18), and taking into account that $\Delta \tau_0(s) = n_{\text{eff}}\Delta L(s)/c$, a simple manipulation gives

$$\tau_{\text{tot}}(s) = \frac{U(s)\Delta \tau_0(s)}{\frac{1}{2}\epsilon_0 n_{\text{eff}}|E_{\text{in}}|^2} = \frac{U(s)\Delta L(s)}{S_{\text{in}}}. \qquad (20)$$

A direct relationship between the local total time delay previously defined and the energy density distribution inside the grating has been derived. Summing up over the grating length according to Eq. (13), the result for the total time spent inside the grating by light is

$$\tau_{\text{tot}} = \sum_s \frac{U(s)\Delta L(s)}{S_{\text{in}}}$$

$$= \frac{\sum_s W(s)}{S_{\text{in}}} = \frac{W}{S_{\text{in}}} = \tau_D, \qquad (21)$$

where $W(s) = U(s)\Delta L(s)$ is the stored energy in layer s and W is the total stored energy. According to the definition given in Ref. [25], τ_D can be identified with the dwell time inside the structure. It has been applied to electron quantum tunneling by Büttiker [26] and extended to optical tunneling by Steinberg [10]. In [27], the dwell time τ_D is well described as "the ratio between the total integrated particle density N in the barrier region divided by the incident current j." In optics, the number of stored photons (i.e., the stored energy W) corresponds to N and the incident photon flux (i.e., the Poynting vector) to j, and Eq. (21) is obtained. The correspondence of the dwell time with the total time delay τ_{tot} computed by the multiple path approach in the small index-contrast limit is an important result. It is an analytical proof of the validity of the proposed multiple path approach in this approximation.

Physically, the dwell time so defined can be related to the time necessary to build up the final photon density in the grating, which under steady state conditions also corresponds to the time to empty the cavity and is related to the cavity Q factor. To our knowledge, this definition has only been applied to the analysis of the entire grating [26,10]. But a local cavity can also be associated with each layer of length $\Delta L(s)$ inside the grating. In Appendix C, the same physical meaning is also attributed to $\tau_D(s) = \tau_{\text{tot}}(s)$, defined for each layer by Eq. (20). Therefore, $\tau_D(s)$ can actually be interpreted as a local dwell time inside the grating.

Despite the formal parallelism between the electron wave function $\Psi(s)$ and the electric field $E(s)$ outlined in [10] and derived from the Schrödinger and Maxwell equations analogy, it must be stressed that Eq. (21) is the correct extension of the dwell time to electromagnetism. Indeed, the energy of an electromagnetic wave is stored in both the electric and magnetic fields. Considering E only (as suggested in Ref. [10]) would produce an extra term related to the self-interference between forward and backward propagating components in Eq. (21), and the agreement and physical insight obtained would be lost.

In Ref. [21], the energy velocity inside each layer was defined as $v_e(s) = S/U(s)$, which after substituting Eqs. (18) and (19) becomes

$$v_e(s) = \frac{c}{n_{\text{eff}}}\frac{1-R_2}{1+R_2} \le \frac{c}{n_{\text{eff}}}. \qquad (22)$$

The local energy velocity is clearly related to the local stored energy and to the Poynting vector $S = S_T$, which is an invariant and represents the energy flux that passes along the structure and is finally transmitted. Equation (22) ensures that the
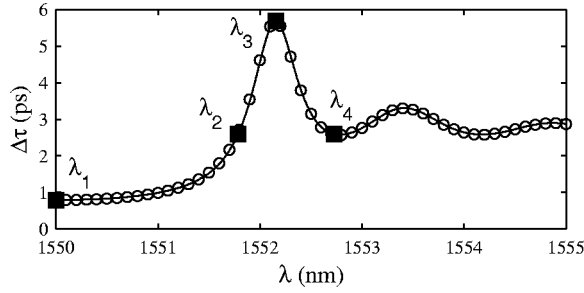
FIG. 4. Time delay spectral characteristic computed using Eq. (13) (circles) and the phase derivative approach (solid line) for a uniform grating with $L=1000\Lambda$, $\delta n=3\times10^{-3}$, $T_{\text{Bragg}}\simeq0.01$, and Bragg wavelength $\lambda_{\text{Bragg}}=1550$ nm. Re$\{\tau_T\}$, Re$\{\tau_R\}$, and τ_{tot} are identical and superimposed. (The time delay evolution in the grating for the four marked wavelengths is described in Fig. 5.)

energy velocity in a periodically perturbed medium is always subluminal, i.e., less than the corresponding velocity in an unperturbed medium c/n_{eff}.

On the contrary, the total time (dwell time) is by no means a time of flight and is not related to any well defined energy transport phenomena. It contains weighted average contributions from all photons present in layer s, regardless of their final state. Therefore, it lacks directionality and any velocity associated with this time definition has no clear physical meaning. As in Ref. [24], a different expression for the local velocity $v_D(s)$ can be introduced using Eq. (21):

$$v_D(s)=\frac{\Delta L(s)}{\tau_D(s)}=\frac{S_{\text{in}}}{U(s)}=\frac{S(s)}{U(s)T_{\text{gr}}}=\frac{v_e(s)}{T_{\text{gr}}}, \qquad (23)$$

which can be shown to be superluminal under certain propagation conditions, namely, for small values of T_{gr}. However, no violation of causality occurs since no real tunneling can be associated with τ_D. This result is in agreement with [28,29], where pulse propagation simulations show that at no time does the intensity of the transmitted pulse exceed the incident intensity in the absence of the grating, i.e., energy is always propagating at subluminal velocity.

III. UNIFORM GRATING SIMULATIONS

The theoretical picture described has been applied to a short and strong uniform grating of length $L=1000\Lambda$, where Λ is the grating period, refractive index modulation $\delta n=3\times10^{-3}$, and transmissivity $T_{\text{Bragg}}\simeq0.01$ at the Bragg wavelength, to allow a reasonably short computational time. As described before, each layer has to be as short as possible in order to be effectively approximated by a nonperturbed region. In the following the grating has been split period by period and the single layer traverse time $\Delta\tau_0(s)$ has been computed taking into account the average refractive index.

Figure 4 shows the real part of the integrated time delay obtained for a wavelength detuning $\Delta\lambda\in[0,5]$ nm with respect to the Bragg wavelength $\lambda_{\text{Bragg}}=1550$ nm. It should be stressed that τ_{tot}, Re$\{\tau_T\}$, and Re$\{\tau_R\}$ are identical and superimposed. The corresponding transfer matrix result [5] is essentially superimposed, as expected from the analytical
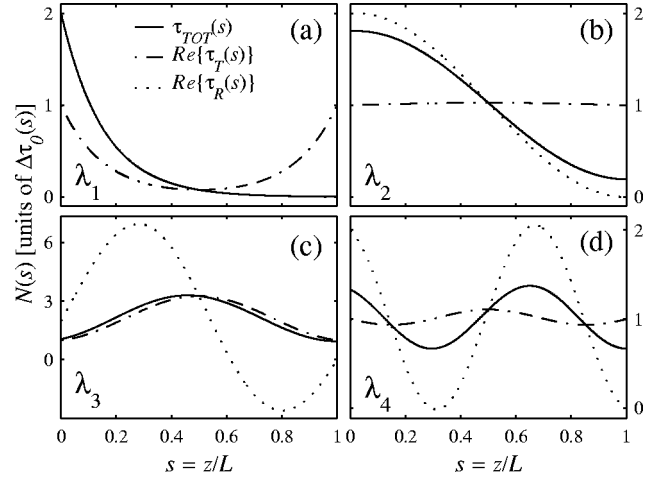

FIG. 5. Longitudinal time delay distribution: $\tau_{\text{tot}}(s)$, solid line; Re$\{\tau_T(s)\}$, dash-dotted line; Re$\{\tau_R(s)\}$, dotted line. The time delays have been normalized to the single pass time delay $\Delta t_0(s)$ and the effective number of passes $N(s)$ is shown. The four wavelengths marked in Fig. 4 are considered: (a) λ_1; (b) λ_2; (c) λ_3; (d) λ_4.

equivalence proved in Appendix B, with minor differences (<0.01 ps) over the whole analyzed bandwidth due to the finite length of each layer.

The main advantage of the proposed approach is the possibility of analyzing the contribution of every single section to the overall time delay. In Fig. 5 the longitudinal distribution of the time delay has been computed for the four wavelengths indicated in Fig. 4, for both transmitted and reflected light and for the layer dwell time. Again, it has to be stressed that the integrated τ_{tot}, Re$\{\tau_T\}$, and Re$\{\tau_R\}$ are identical, despite the different spatial distributions. For the sake of clarity, an effective number of passes $N(s)$ in the selected layer s is shown in Fig. 5, where

$$N_T(s)=\frac{\text{Re}\{\tau_T(s)\}}{\Delta\tau_0(s)}, \qquad N_R(s)=\frac{\text{Re}\{\tau_R(s)\}}{\Delta\tau_0(s)}. \qquad (24)$$

Intuitively, the local time delay is expected to depend on the single pass time delay $\Delta\tau_0(s)$ and on the average number of passes N, since the layer is considered as a nonscattering region and N accounts for the multiple reflections in the effective cavity. This can easily be visualized in Figs. 3(a) and 3(b).

It is worth pointing out that the number of passes at the grating ends ($z=0$ and L) is always fixed irrespective of the wavelength, since no multiple reflections occur (the associated effective cavity has $\rho=0$). Transmitted light simply crosses these layers once during propagation toward the end of the grating $[N_T(0)=N_T(L)=1]$. Reflected light always passes twice through the very beginning of the grating [it enters the grating and is finally bounced back, $N_R(0)=2$], while it never reaches the very end $[N_R(L)=0]$ since otherwise it would never be reflected. These general relations can be derived analytically from the corresponding Eqs. (9)–(11) in the limits $z=sL\rightarrow0,L$.

The Bragg wavelength (λ_1) is presented in Fig. 5(a), while Fig. 5(c) shows the evolution at a wavelength corresponding to the time delay maximum and close to the first transmission resonance (λ_3). As expected, $\tau_{\text{tot}}(s) \simeq \text{Re}\{\tau_R(s)\}$ when $R_{\text{gr}} \simeq 1$ and $\tau_{\text{tot}}(s) \simeq \text{Re}\{\tau_T(s)\}$ when $T_{\text{gr}} \simeq 1$. At the Bragg wavelength, the dwell time decays exponentially along the structure in accordance with the evanescent propagation at this wavelength. Almost all the energy is stored in the first part of the grating. At the transmission resonance, instead, much higher energy storage is achieved, since light is trapped in the grating center between two highly reflective mirrors and constructive interference between different paths takes place. Figures 5(b) and 5(d) refer to wavelengths λ_2 and λ_4 which have the same overall time delay $\tau = 2.75$ ps. However, the different scattering conditions produce a completely different distribution of delay inside the structure and, therefore, different energy density distributions. It is already apparent that each wavelength "sees" the grating in a different way. This particular mapping can potentially be used to characterize the grating along its length, to design different devices, or to understand the spectral response differences under various perturbations and noise distributions.

Considering the transmission time delay, inside the band gap [for $\lambda = \lambda_1$, Fig. 5(a)] the light that passes through the grating is mainly delayed at the edges of the structure. It can be shown that at this wavelength the multiple paths $|\psi_{T,k}(s)\rangle$ are interfering destructively for all layers s. Around the grating center, the destructive interference is almost complete due to sufficient contributions from either side of the layer. It actually gets more complete as the grating reflectivity increases, since the number of interfering paths increases. Therefore, the corresponding time delay distribution goes asymptotically to zero. As the grating edges are approached, however, the contributing paths are predominantly only from one side and the destructive interference becomes gradually incomplete. The time delay distribution at the grating ends is therefore always finite. This picture is confirmed by comparing the time delay of different strength gratings, as shown in Fig. 6. The higher the reflectivity, the lower the transmission time delay in the structure center [Fig. 6(a)], so that the integrated traversal time decreases for increasing grating strength [Fig. 6(b)]. This phenomenon is typical of structures with tunneling and/or evanescent wave propagation and it is known as the "Hartman effect" [30]. In sufficiently strong gratings [$R \gtrsim 0.7$ in Fig. 6(b)], this effect produces a transmission time delay that is actually shorter than the one in vacuum. Transmission under these circumstances has been interpreted as "superluminal" [31,14,28]. In pulse transmission through periodic structures, it has been well established that "superluminal" effects are associated with lack of sufficient destructive interference at the leading edge of the pulse and strong destructive interference during the main duration of the pulse [15,14]. On the other hand, the picture presented shows that the Hartman effect and the associated superluminal effect under steady state conditions are due to strong and nearly complete destructive interference at the central part of the periodic structure and partial interference near its edges.
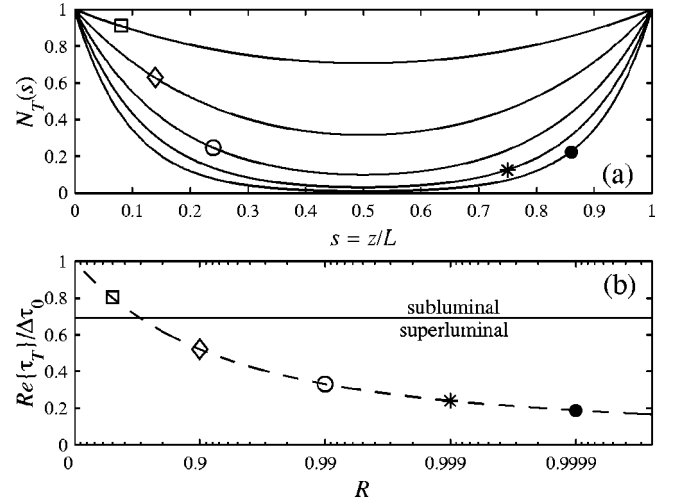

FIG. 6. Transmission time delay distributions (a) and integrated time delay (b) at the Bragg wavelength λ_1 for different strength gratings: $\square$ $R = 0.5$; $\diamond$ $R = 0.9$; $\bigcirc$ $R = 0.99$; $\ast$ $R = 0.999$; $\bullet$ $R = 0.9999$. In (a) the effective number of passes $N_T(s)$ is shown in units of $\Delta\tau_0(s)$. In (b) the integrated time delay $\text{Re}\{\tau_T\}$ (dashed line) is normalized to the single pass time delay $\Delta\tau_0 = n_{\text{eff}}L/c$. The solid line shows the traverse time in vacuum.

Outside the band gap [for $\lambda = \lambda_3$ and $\lambda = \lambda_4$, Figs. 5(c) and 5(d)], the cavity round-trip reflectivity $|\rho|^2 = R_1 R_2$ oscillates along the structure. Different paths interfere constructively close to transmission resonances and destructively near transmissivity minima. Oscillating time delay contributions are therefore obtained.

The reflection time delay does not allow a simple physical interpretation. Qualitatively, Fig. 5 shows that inside the band gap $\text{Re}\{\tau_R(s)\}$ is always positive, while as soon as the wavelength λ moves outside the gap it can be shown that it becomes negative in certain layers. In particular, it may assume very high positive and negative values close to reflectivity minima, as shown for the case of $\lambda = \lambda_3$. Again, this nonintuitive behavior is related to interference effects. Considering Fig. 3(b), it is clear that the reflected component $|\psi_{R,0}(s)\rangle$ does not contribute to the time delay directly but only through interference at the beginning of the grating with the other contributing paths. The real part of this interference contribution can be negative in general, keeping in mind the nonorthogonality of the field components $|\psi_{R,k}(s)\rangle$, and can produce a negative reflection time delay in the layer. Pulse propagation gives an intuitive explanation of this steady state result. Negative time delays are associated with a reflected pulse peak originating mainly in the leading edge of the incident pulse. Therefore, the reflected peak leaves the considered layer before the incident peak actually enters it [32].

IV. TIME DELAY DISTRIBUTION: GRATINGS WITH SMALL PERTURBATIONS

The most commonly accepted approach to an operative definition of time delay is to correlate the time spent by light in a certain region to the change in a physical quantity induced by an external perturbation, when a direct and linear

relation can be inferred between such a change and the time of interaction. This approach originated from the problem of measuring the duration of quantum-mechanical collisions and was first applied to the traversal time for particle tunneling by Büttiker and Landauer [33]. Different external perturbations have been proposed in quantum mechanics (oscillating barrier [33], time-modulated incident wave [34], Larmor precession of spin [26]), and applied later in optics (introduction of lossy layers [18], Faraday rotation [35]). The common characteristic of the perturbation analysis is to obtain complex-valued interaction times, in which the real part can be directly related to the classical time delay. In the following, the same kind of analysis will be applied to a localized region inside the grating, in close similarity to the Steinberg approach [18]. It will be shown that clear physical meaning is associated with both the real and imaginary parts of the local time delay obtained by the multiple path technique.

Let us introduce an infinitesimal phase perturbation $d\phi$ in a defined position s inside the grating. This kind of perturbation can easily be introduced in a grating by localized heating or strain, its effect is reversible, and experimental verification of the simulated time delay distributions can be obtained by simply scanning the grating. For these reasons the insertion of a phase defect seems particularly attractive and will be directly analyzed. Analogous results can be derived by using other proposed perturbation schemes (local variation of layer losses or local perturbation with an external magnetic field), taking into account the different physical quantities associated with them.

Using the Sec. II B formalism and Eq. (7b), the transmission coefficient t is given by

$$t_{\text{pert}}(s) = \frac{t_1 + t_2 e^{jd\phi}}{1 - \rho_0 e^{j2d\phi}}, \tag{25a}$$

$$t_{\text{gr}}(s) = \frac{t_1 + t_2}{1 - \rho_0} \tag{25b}$$

for the perturbed and unperturbed structures, respectively. In the unperturbed grating $d\phi = 0$ and from Eq. (6) $\rho_0 = r_{1-}r_2$. Using the Taylor expansions for $d\phi \to 0$ in the previous expressions, after a lengthy manipulation it is possible to write

$$\frac{t_{\text{pert}}(s)}{t_{\text{gr}}(s)} \simeq e^{jd\phi(1+\rho_0)/(1-\rho_0)} \simeq e^{jd\phi\tau_T(s)/\Delta\tau_0(s)}, \tag{26}$$

where $\rho_0 \simeq \rho = r_{1-}r_2 e^{j2d\phi}$ for an infinitesimal perturbation. The reflection coefficient computation is similar, but mathematically more involved. From Eq. (8b) and using the same approximations as before,

$$\frac{r_{\text{pert}}(s)}{r_{\text{gr}}(s)} \simeq e^{j2d\phi[T_1/(1-\rho_0)]\rho_0/(\rho_0-R_1)} \simeq e^{jd\phi\tau_R(s)/\Delta\tau_0(s)}. \tag{27}$$

It is analytically confirmed that the effect of the perturbation can be directly related to the complex time delays (9) and (10).

Taking into account that the derived time delays are complex valued, the effect of the perturbation can be further analyzed. Considering a generic final transmission or reflection coefficient $f = t, r$ and remembering that $d\phi/\Delta\tau_0(s) = \omega_0$,

$$f_{\text{pert}}(s) = f_{\text{gr}}(s)e^{jd\phi\tau_f(s)/\Delta\tau_0(s)} = f_{\text{gr}}(s)e^{j\omega_0\tau_f(s)}$$

$$= f_{\text{gr}}(s)e^{j\omega_0\,\text{Re}\{\tau_f(s)\}}e^{-\omega_0\,\text{Im}\{\tau_f(s)\}}.$$

Using $F_{\text{pert}}(s) \simeq F_{\text{gr}} + \Delta F$, where $F = |f|^2 = T, R$ refers to either transmissivity or reflectivity, it is easy to show that $\ln[F_{\text{pert}}(s)/F_{\text{gr}}] \simeq \Delta F/F_{\text{gr}}$ and therefore

$$\Delta\phi_f(s) = \omega_0\,\text{Re}\{\tau_f(s)\}, \tag{28}$$

$$\Delta F(s) \simeq -2\omega_0 F_{\text{gr}}\,\text{Im}\{\tau_f(s)\}, \tag{29}$$

where $\Delta F = \Delta T, \Delta R$ are the transmissivity and reflectivity variations, respectively. Therefore both real and imaginary parts of the transmission and reflection time delays have a precise physical meaning. Introducing a phase perturbation results in a phase change related to the real part of the time delay, while the amplitude change is related to the corresponding imaginary part. They are directly related to measurable variations in the transmission and reflection coefficients. Using Eq. (29), it is quite straightforward to show that Eq. (12b) results in $\Delta T + \Delta R = 0$, which is consistent with the energy conservation principle.

Equation (28) can also be derived from Eq. (24) using intuitive arguments. The more times light crosses the layer s where the perturbation is located, the bigger phase shift is accumulated, so that $\Delta\phi(s) = d\phi N(s)$ where $N(s)$ is the effective number of passes in the layer.

The analysis developed by Steinberg [36,18] gives a theoretical interpretation of the effect described, using the theory of ''weak measurements'' developed by Aharonov and Vaidman [37]. In a classical quantum measurement theory, it is not possible to get information both about the time spent by light in a certain region and about the final transmitted or reflected state. The first measurement collapses the system status on the measured eigenstate and thus the system evolution is irreversibly altered. But if the measurement is sufficiently ''gentle'' (but therefore imprecise), the system does not collapse and both pieces of information (i.e., the weak value of the time delay) can be obtained by averaging a large set of such measurements. The final result is in general a complex number. The real part is related to the mean variation in the measured quantity (''pointer'') and gives the final result of the measurement. The imaginary part is shown to be associated with the mean shift in the pointer conjugate momentum, which corresponds to the back action of the measurement on the system. It can be thought of as a measure of how much the system has been perturbed.

According to the above definition, the perturbation scheme proposed in this section is a weak measurement. The optical phase of light is the measurement pointer since the phase shift induced by the perturbed layer is used as a clock. The conjugate momentum is represented by the photon number, i.e., the transmissivity and reflectivity of the grating. The
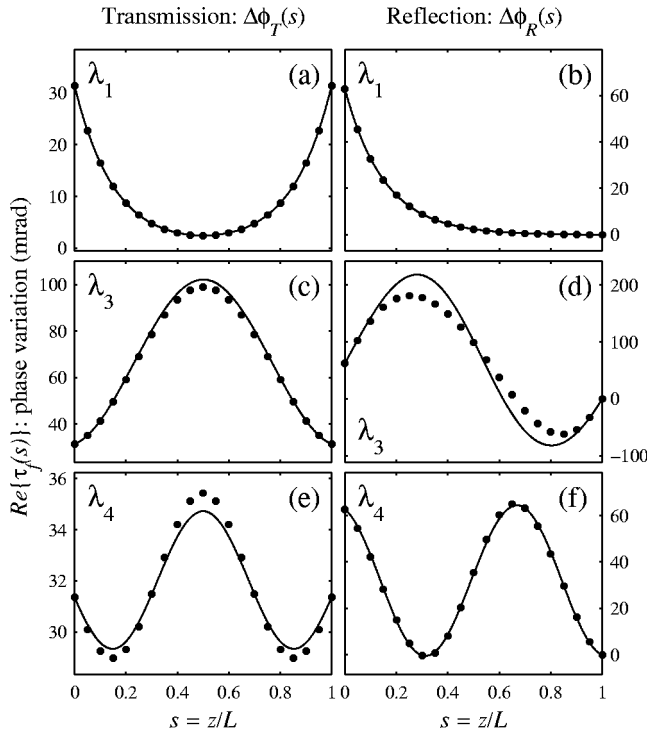
FIG. 7. Transmission (left column) and reflection (right column) phase variations induced by a $\Lambda/100$-long layer added to the grating (in mrad). A uniform grating with $L=1000\Lambda$, $\delta n=3\times10^{-3}$, and $\lambda_{\text{Bragg}}=1550$ nm has been simulated. The three different wavelengths shown in Fig. 4 are represented: λ_1 (upper row), Bragg wavelength; λ_3 (central row), transmission resonance; λ_4 (lower row), first reflection sidelobe. Both the simulated $\Delta\phi(s)$ (filled circles) and the values obtained from the real part of the time delay distributions and Eq. (28) (solid lines) are shown.
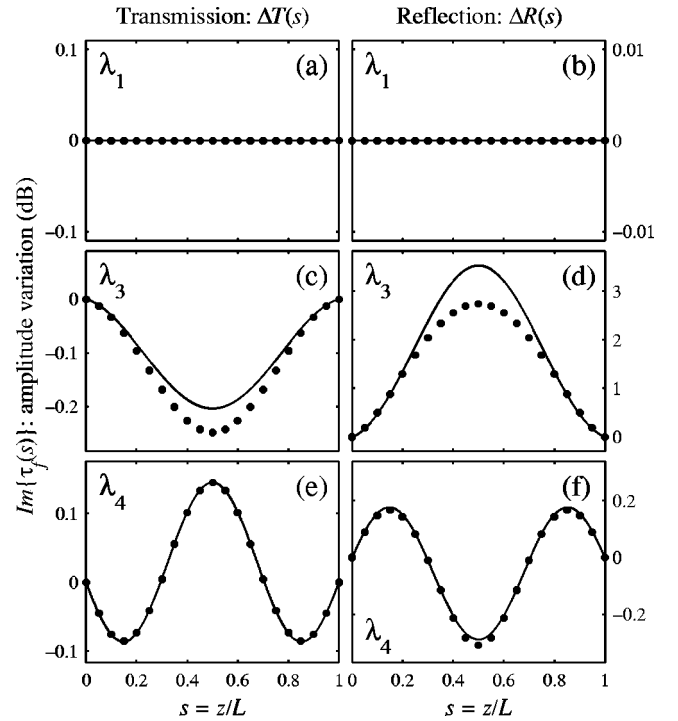

FIG. 8. Transmissivity (left column) and reflectivity (right column) variation (in dB) induced by the inclusion of a $\Lambda/100$-long layer in the grating. The simulated grating is uniform with $L=1000\Lambda$, $\delta n=3\times10^{-3}$, and $\lambda_{\text{Bragg}}=1550$ nm. λ_1 (upper row), Bragg wavelength; λ_3 (central row), transmission resonance; λ_4 (lower row), first reflection sidelobe. Both the values obtained from grating simulations (filled circles) and from the imaginary part of the time delay distributions (29) (solid lines) are shown.

variations ΔT and ΔR can be interpreted as the effects of the perturbation introduced in the system by the measurement and are proportional to the time delay imaginary part. This theoretical approach also shows that correct results are obtained as long as the state of the system remains to a large extent undisturbed by the measuring procedure. Therefore, good agreement between the complex time delay distributions calculated with Eqs. (9) and (10) and the effect of a localized phase defect is expected where $\text{Im}\{\tau(s)\}$ is small, while differences are expected when the perturbation significantly affects the grating. This is the case of a relatively strong perturbation or a weak or strong perturbation near the transmission resonances.

This approach has been numerically tested on the uniform grating already described in Sec. III ($L=1000\Lambda$, $\delta n=3\times10^{-3}$). A $\Lambda/100$-long nonscattering layer has been added to the grating in different positions ($0L,0.05L,0.1L,\ldots,L$), resulting in $d\phi=\pi/100\approx31$ mrad. The small $d\phi$ value is necessary to guarantee the weak measurement assumption. The corresponding transmission and reflection phase variations $\Delta\phi(s)$ are shown in Fig. 7 (filled circles) and are compared with the corresponding distributions obtained from the local time delay and Eq. (28) (solid lines). Three representative wavelengths are considered (see Fig. 4): λ_1, Bragg wavelength; λ_3, time delay maximum (close to the transmis-

sion resonance $T_{\text{gr}}=1$); λ_4, time delay minimum (first reflection sidelobe). In Fig. 8, the amplitude variations (in dB) corresponding to the $\Lambda/100$-long defect inclusion are shown in both transmission (left column) and reflection (right column). Again, filled circles represent the perturbed grating simulations and solid lines the results of time delay analysis given by Eq. (29).

In transmission, Figs. 7(a) and 7(b) show that at the Bragg wavelength λ_1 the agreement is almost perfect, and much smaller phase variations are obtained in the center of the grating with respect to the sides. The experimental detection of such a phase shift decrease can give direct evidence of shorter interaction times of light in a periodic structure compared to free space propagation. Possibly, a direct proof of superluminal time of flight can be found in a sufficiently strong grating. In reflection the perturbation effect decays almost exponentially along the grating length. As commented with respect to Fig. 5, it closely follows the local power distribution, since light is mainly reflected in the first section and cannot sample the end of the structure.

This intuitive (but approximate) interpretation was first proposed in Ref. [38], where the reflection phase shift was related to the power distribution inside the grating. Good fitting was obtained for wavelengths inside the band-gap region, but worse agreement was found close to the band-gap edge. The approach presented here explains the limits of that

analysis and extends those results. Close correspondence between the reflection time delay and power evolution is found inside the band gap, since $\tau_R(s) \simeq \tau_{tot}(s) \propto U(s)$ for $R \simeq 1$, as shown in Fig. 5(a) and Eq. (21). But further away from the Bragg condition the existence of two different final states becomes important and the above approximation fails. Instead, the application of the local time delay distribution gives good agreement even outside the band gap (λ_3 and λ_4, central and lower rows in Fig. 7), and it can be applied to both reflected and transmitted light independently.

The nonperfect fit obtained for λ_3 and λ_4 is consistent with the weak measurement theory. At the Bragg wavelength λ_1 (upper row), Figs. 8(a) and 8(b) show that the induced perturbation is negligible and excellent agreement between time delay computation and perturbation analysis is expected. Close to the first reflection sidelobe λ_4 and in particular to the first transmission resonance λ_3, much bigger perturbations of the grating are obtained compared to the Bragg wavelength, and a worse agreement between theory and measurement is therefore expected. It is apparent that the smoother the transmission and reflection spectra around the considered wavelength, the less any small variation affects the final shape, and thus the better the time delay distribution can be inferred from this kind of measurement. It is obvious that further reducing the phase shift amplitude improves the fit that can be obtained at all wavelengths. But it has been numerically verified that a good measurement of the theoretical time delay distribution at λ_3 requires $d\phi$ as small as $\pi/500$, which is not experimentally feasible.

Nevertheless, Fig. 7(d) clearly shows that for $\lambda = \lambda_3$ the experimental detection of positive phase shifts at the grating far end ($z \to L$) can be correlated with the nonintuitive idea of negative interaction times of light in the perturbed region.

V. CONCLUSIONS

A method for local time delay characterization of periodic scattering structures such as gratings has been developed. The grating is divided into small layers which can be considered as free space regions. A multiple reflection approach is used to calculate all the possible classical paths for both transmitted and reflected light. This effective Fabry-Pérot analysis allows a field decomposition in terms of components whose traversal time inside the layer is well defined, and the average time spent in the layer by transmitted or reflected light can be evaluated. A generally complex-valued time is obtained, but clear physical meaning has been given to both its real and imaginary parts. The real part is related to the actual traversal time, while the imaginary part gives the extent of the back action of the measurement on the system. Finally, the dwell time in the structure is derived by appropriately weighting and summing up the two contributions. The dwell time is analytically shown to be always real, positive, and directly related to the power distribution inside the grating in small index-contrast gratings.

The reflection and transmission time delays of a uniform grating derived with this approach have been proved to agree with those from standard techniques based on transfer matrix calculations and phase derivatives. A possible measurement

technique to obtain an experimental confirmation of the computed results has been discussed, with particular interest in superluminal propagation and negative time delay verification. Scanning a small phase shift along the grating has been shown to produce a variation of the output optical phase and power proportional to the real and imaginary parts of the local time delay, respectively. An experimental demonstration of the proposed technique has been reported elsewhere [39] with respect to the time delay imaginary part.

The proposed theoretical model may prove to be a useful tool in the design of active devices (in cold cavity conditions) and dispersion compensating gratings [8]. The point-by-point analysis of the grating features can also be effective in investigating local defects contribution in gratings (i.e. unwanted phase shifts in standard writing techniques) or robustness analysis of non-standard grating design. The results of Sec. IV can also be used to understand the effect of distributed phase errors on the reflectivity and time delay spectra of Bragg gratings [40]. Such a detailed analysis will be the subject of another publication.

APPENDIX A: DERIVATION OF TIME DELAY EXPRESSIONS

In the following a monochromatic excitation $|\psi_{in}\rangle \to E_{in} = e^{j(\beta z - \omega_0 \xi)}$ will be considered. Using the Eq. (1) formalism and considering the time delay as a generic complex number, Eq. (7b) allows the transmission delay computation:

$$\langle \psi_T | \psi_T \rangle = \frac{|t_{1+}t_2|^2}{|1-\rho|^2} = T_{gr}, \tag{A1a}$$

$$\langle \psi_T | \hat{\tau}_T(s) | \psi_T \rangle = \frac{t_{1+}^* t_2^* e^{-j\phi}}{1 - r_{1-}^* r_2^* e^{-j2\phi}} \sum_{k=1}^{\infty} (2k-1) \Delta\tau_0(s)$$
$$\times t_{1+}t_2 e^{j\phi} [r_{1-}r_2 e^{j2\phi}]^{k-1}$$
$$= \frac{|t_{1+}t_2|^2}{1-\rho^*} \Delta\tau_0(s) \frac{1+\rho}{[1-\rho]^2}, \tag{A1b}$$

where $\rho = r_{1-}r_2 e^{j2\phi}$ is the round-trip reflection coefficient (6) and $\tau_{T,k}(s) = (2k-1)\Delta\tau_0(s)$ is the time delay for each field component $|\psi_{T,k}(s)\rangle$. $\Delta\tau_0(s)$ is the time spent in the layer in a single pass and $(2k-1)$ is the number of passes before the photon is transmitted, as shown in Fig. 3(a). Combining Eqs. (A1a) and (A1b) according to Eq. (1), the expression for the transmission time delay $\tau_T(s)$ in layer s is

$$\tau_T(s) = \frac{\langle \psi_T | \hat{\tau}_T(s) | \psi_T \rangle}{\langle \psi_T | \psi_T \rangle} = \Delta\tau_0(s) \frac{1+\rho}{1-\rho}. \tag{A2}$$

In general, $\tau_T(s)$ is a complex number whose real and imaginary parts can be expressed as follows:

$$\text{Re}\{\tau_T(s)\} = \Delta\tau_0(s)T_{\text{gr}}\frac{1-R_1R_2}{T_1T_2}, \tag{A3a}$$

$$\text{Im}\{\tau_T(s)\} = 2\Delta\tau_0(s)\text{Im}\{\rho\}\frac{T_{\text{gr}}}{T_1T_2}, \tag{A3b}$$

where T_1, R_1 and T_2, R_2 are the transmissivity and reflectivity of the left and right reflectors, respectively. Equation (A3a) shows that the real part of the transmission time delay is always positive.

With an analogous derivation starting from Eq. (8b) the reflection time delay $\tau_R(s)$ can be computed:

$$\langle\psi_R|\psi_R\rangle = |r_{\text{gr}}|^2 = R_{\text{gr}} = (1-T_{\text{gr}}), \tag{A4a}$$

$$\langle\psi_R|\hat\tau_R(s)|\psi_R\rangle = r_{\text{gr}}^*\left[r_{1+}0 + \sum_{k=1}^{\infty}2k\Delta\tau_0(s)\right.$$

$$\left.\times t_{1+}t_{1-}r_2e^{j2\phi}[r_{1-}r_2e^{j2\phi}]^{k-1}\right]$$

$$= r_{\text{gr}}^*2\Delta\tau_0\frac{t_{1+}t_{1-}r_2e^{j2\phi}}{[1-\rho]^2}. \tag{A4b}$$

$|\psi_{R,0}(s)\rangle$ is reflected before reaching layer s and therefore $\tau_{R,0}(s)=0$, while all the other components pass $2k$ times through s [see Fig. 3(b)]. The desired expression is

$$\tau_R(s) = \frac{\langle\psi_R|\hat\tau_R(s)|\psi_R\rangle}{\langle\psi_R|\psi_R\rangle}$$

$$= 2\Delta\tau_0(s)\frac{r_{\text{gr}}^*(t_{1+}t_{1-}r_2e^{j2\phi})/[1-\rho]^2}{|r_{\text{gr}}|^2}. \tag{A5}$$

With algebraic manipulation and using the reciprocity relation $r_{1+}/t_{1+} = -r_{1-}^*/t_{1+}^*$ valid in the lossless case [19], Eq. (A5) can be simplified as follows:

$$\tau_R(s) = 2\Delta\tau_0(s)\frac{T_1}{1-\rho}\frac{\rho}{\rho-R_1}. \tag{A6}$$

The corresponding real and imaginary parts are found to be

$$\text{Re}\{\tau_R(s)\} = \Delta\tau_0(s)\frac{T_{\text{gr}}}{T_1T_2}\left[1-R_1R_2+\frac{R_2-R_1}{R_{\text{gr}}}\right], \tag{A7a}$$

$$\text{Im}\{\tau_R(s)\} = -2\Delta\tau_0(s)\text{Im}\{\rho\}\frac{T_{\text{gr}}}{T_1T_2}\frac{T_{\text{gr}}}{R_{\text{gr}}}. \tag{A7b}$$

The total time $\tau_{\text{tot}}(s)$ spent in section s by a photon is given by the average value of $\tau_T(s)$ and $\tau_R(s)$, weighted by the final state probability T_{gr} or R_{gr}. After an algebraic manipulation its concise expression results:

$$\tau_{\text{tot}}(s) = \tau_T(s)T_{\text{gr}} + \tau_R(s)R_{\text{gr}}$$

$$= \Delta\tau_0(s)T_{\text{gr}}\frac{1+R_2}{1-R_2}, \tag{A8}$$

where the relations $|\rho|^2 = R_1R_2$ and $R_{\text{gr}} = |R_1-\rho|^2/|1-\rho|^2R_1$ [easily derived from the reflection coefficient r_{gr} definition (8b)] have been used.

APPENDIX B: $\text{Re}\{\tau_f\} = \tau_{\text{phase}}$ IN UNIFORM GRATINGS: ANALYTIC PROOF

The equivalence between the multiple path approach and the classical phase time delay $\tau_{\text{phase}} = \partial\theta/\partial\omega$ [3] can be analytically proved only in the special case of a uniform grating.

Taking into account the former approach and layers of infinitesimal length dz, the single pass time delay is $\Delta\tau_0 = n_{\text{eff}}dz/c$ and the summation in Eq. (13) has to be replaced by integration over the grating length L. If the transmission time delay $\text{Re}\{\tau_T\}$ is considered, it is convenient to express Eq. (A3a) in terms of the left and right reflector transmissivities $T_1(z)$ and $T_2(z)$:

$$\text{Re}\{\tau_T\} = \int_0^L \frac{n_{\text{eff}}}{c}T_{\text{gr}}\frac{T_1(z)+T_2(z)-T_1(z)T_2(z)}{T_1(z)T_2(z)}dz. \tag{B1}$$

The generic transmissivity T for a uniform grating of length Δ is given by [3]

$$T = |t|^2 = \frac{(\gamma/\kappa)^2}{\cosh^2(\gamma\Delta)-(\hat\sigma/\kappa)^2}, \tag{B2}$$

where $\Delta = L, z, (L-z)$ for $T_{\text{gr}}, T_1(z), T_2(z)$, respectively, $\hat\sigma$ is the effective detuning from the Bragg wavelength, κ is the grating coupling constant, and $\gamma = \sqrt{\kappa^2-\hat\sigma^2}$ [3]. The integration of Eq. (B1) gives the following expression for the integrated transmission time delay:

$$\text{Re}\{\tau_T\} = \frac{n_{\text{eff}}L}{c}\frac{[\sinh(2\gamma L)]/2\gamma L-(\hat\sigma/\kappa)^2}{\cosh^2(\gamma L)-(\hat\sigma/\kappa)^2}. \tag{B3}$$

If the reflection time delay $\text{Re}\{\tau_R\}$ is considered, the integration of Eq. (A7a) over the grating length L gives

$$\text{Re}\{\tau_R\} = \text{Re}\{\tau_T\} + \frac{n_{\text{eff}}}{c}\frac{T_{\text{gr}}}{R_{\text{gr}}}\int_0^L\frac{R_2(z)-R_1(z)}{T_1(z)T_2(z)}dz, \tag{B4}$$

where $R_1(z)$ and $R_2(z)$ are the reflectivities of the left and right reflectors. The integrand function in Eq. (B4) is an odd function with respect to $z=L/2$, since $T_1(z)=T_2(L-z)$ and $R_1(z)=R_2(L-z)$ in a symmetric structure. Therefore the integral is equal to 0 and

$$\text{Re}\{\tau_R\} = \text{Re}\{\tau_T\}. \tag{B5}$$

Finally, it is straightforward from Eq. (A8) to show that even $\tau_{\text{tot}} = \text{Re}\{\tau_T\}$.

The derivation of the phase time delay is algebraically more involved. Starting from the analytic expression of the coefficients t_{gr} and r_{gr} of a uniform grating [3], it is easy to recognize that the transmission and reflection phases θ_T and θ_R are equal apart from a constant factor. Therefore, the corresponding transmission and reflection time delays $\tau_{phase} = \partial \theta_f / \partial \omega$ are equal and equal to the total time delay, as is clear from Eq. (11). The corresponding expression is

$$\tau_{phase} = \frac{\partial}{\partial \omega} \left\{ \arctan \left[\frac{\hat{\sigma}}{\gamma} \tanh(\gamma L) \right] \right\}. \tag{B6}$$

Performing the differentiation and taking into account that $\partial \hat{\sigma} / \partial \omega = n_{eff}/c$, the total time delay is found to be [41]

$$\text{Re}\{\tau_R\} = \frac{n_{eff} L}{c} \frac{[\sinh(2\gamma L)]/2\gamma L - (\hat{\sigma}/\kappa)^2}{\cosh^2(\gamma L) - (\hat{\sigma}/\kappa)^2}. \tag{B7}$$

The equivalence between τ_{tot}, $\text{Re}\{\tau_T\}$, $\text{Re}\{\tau_R\}$, and τ_{phase} at every wavelength is analytically proved by Eqs. (B3) and (B7). It has to be noted that the average refractive index n_{eff} has been used and the longitudinal modulation $n_{eff}(z)$ has been disregarded in this derivation. Therefore, the analytical results presented are valid in the small index-contrast approximation only (see Sec. II C).

APPENDIX C: LOCAL DWELL TIME DERIVATION AND PHYSICAL INTERPRETATION

The dwell time τ_D associated with a generic cavity can be interpreted as the time necessary to empty the cavity itself in steady state conditions. The same physical meaning can be extended to the local dwell time $\tau_D(s) = \tau_{tot}(s)$ introduced by Eq. (20) by considering a generic layer s of length $\Delta L(s)$ and the associated Fabry-Pérot cavity. The stored energy is $U(s)\Delta L(s)$ and the flux leaving the layer is given by $S_{out}(s) = S_+(s) + S_-(s)$, where both the counterpropagating fields $E_+(s)$ and $E_-(s)$ given by Eq. (16) are considered. But $S_{out}(s)$ takes into account even photons that will be scattered during the propagation and will reenter layer s. This means that these photons do not actually contribute to energy removal from the analyzed layer and therefore must not be accounted for in the dwell time computation. The fields associated with photons that will not be further scattered and reenter the layer s are therefore

$$\widetilde{E}_+(s) = E_+(s) t_2 = E_T, \tag{C1a}$$

$$\widetilde{E}_-(s) = E_-(s) t_{1-} + E_{in} r_{1+} = E_R, \tag{C1b}$$

and correspond to the transmitted and reflected fields, as is easily verified from Eqs. (7b), (8b), and (16). It is worth noting that interference in the backward direction between photons leaving section s and photons scattered back before reaching s has to be considered. Using Eq. (C1) and considering the correct Poynting vector fluxes, the outgoing associated flux $\widetilde{S}_+(s) + \widetilde{S}_-(s) = S_T + S_R$ is constant, independent of the layer position, and equal to S_{in} because of energy conservation. Therefore, applying the general definition of dwell time to each layer, the local dwell time $\tau_D(s)$ is

$$\tau_D(s) = \frac{U(s)\Delta L(s)}{\widetilde{S}_+ + \widetilde{S}_-} = \frac{W(s)}{S_{in}}, \tag{C2}$$

and the formal relation introduced in Eqs. (20) and (21) is proved.

[1] P. Yeh, A. Yariv, and C. S. Hong, J. Opt. Soc. Am. **67**, 423 (1977).

[2] J. M. Bendickson, J. P. Dowling, and M. Scalora, Phys. Rev. E **53**, 4107 (1996).

[3] T. Erdogan, J. Lightwave Technol. **15**, 1277 (1997).

[4] A. Yariv, IEEE J. Quantum Electron. **9**, 919 (1973).

[5] M. Yamada and K. Sakuda, Appl. Opt. **26**, 3474 (1987).

[6] P. Yeh, *Optical Waves in Layered Media* (Wiley, New York, 1988).

[7] S. Wang, IEEE J. Quantum Electron. **10**, 413 (1974).

[8] F. Ouellette, Opt. Lett. **12**, 847 (1987).

[9] R. Y. Chiao and A. M. Steinberg, in *Progress in Optics*, edited by E. Wolf (Elsevier, Amsterdam, 1997), Vol. 37, pp. 345–405.

[10] A. M. Steinberg and R. Y. Chiao, Phys. Rev. A **49**, 3283 (1994).

[11] S. Y. Zhu, N. H. Liu, H. Zheng, and H. Chen, Opt. Commun. **174**, 139 (2000).

[12] G. B. Morrison and D. T. Cassidy, IEEE J. Quantum Electron. **36**, 633 (2000).

[13] R. P. Feynman, R. B. Leighton, and M. Sands, *The Feynman Lectures on Physics* (Addison-Wesley, Reading, MA, 1965), Vol. III.

[14] Y.-P. Wang and D.-I. Zhang, Phys. Rev. A **52**, 2597 (1995).

[15] Y. Japha and G. Kurizki, Phys. Rev. A **53**, 586 (1996).

[16] J. Y. Lee, H. W. Lee, and J. W. Hahn, J. Opt. Soc. Am. B **17**, 401 (2000).

[17] D. Sokolovski and J. N. L. Connor, Phys. Rev. A **47**, 4677 (1993).

[18] A. M. Steinberg, Phys. Rev. A **52**, 32 (1995).

[19] S. A. Furman and A. V. Tikhonravov, *Optics of Multilayer Systems* (Editions Frontières, Gif-sur-Yvette, France, 1992).

[20] R. P. Feynman and A. R. Hibbs, *Quantum Mechanics and Path Integrals* (McGraw-Hill, New York, 1965).

[21] A. Yariv and P. Yeh, J. Opt. Soc. Am. **67**, 438 (1977).

[22] H. Kogelnik, in *Integrated Optics*, edited by T. Tamir (Springer-Verlag, Berlin, 1979), p. 67.

[23] J. E. Sipe and G. Stegeman, J. Opt. Soc. Am. **69**, 1676 (1979).

[24] G. D'Aguanno, M. Centini, M. Scalora, C. Sibilia, M. J. Bloemer, C. M. Bowden, J. W. Haus, and M. Bertolotti, Phys. Rev. E **63**, 036610 (2001).

[25] F. T. Smith, Phys. Rev. **118**, 349 (1960).

[26] M. Büttiker, Phys. Rev. B **27**, 6178 (1983).

[27] M. Büttiker, in *Electronic Properties of Multilayers and Low-Dimensional Semiconductor Structures*, edited by J. M. Cham-

berlain, L. Eaves, and J. C. Portal (Plenum, New York, 1990), pp. 297–315.

[28] F. Schreier, M. Schmitz, and O. Bryngdahl, Opt. Commun. **163**, 1 (1999).

[29] M. Scalora, J. P. Dowling, A. S. Manka, C. M. Bowden, and J. W. Haus, Phys. Rev. A **52**, 726 (1995).

[30] T. E. Hartman, J. Appl. Phys. **33**, 3467 (1962).

[31] A. M. Steinberg, P. G. Kwiat, and R. Y. Chiao, Phys. Rev. Lett. **71**, 708 (1993).

[32] J. Peatross, S. A. Glasgow, and M. Ware, Phys. Rev. Lett. **84**, 2370 (2000).

[33] M. Büttiker and R. Landauer, Phys. Rev. Lett. **49**, 1739 (1982).

[34] M. Büttiker and R. Landauer, Phys. Scr. **32**, 429 (1985).

[35] V. Gasparian, M. Ortuño, J. Ruiz, and E. Cuevas, Phys. Rev. Lett. **75**, 2312 (1995).

[36] A. M. Steinberg, Phys. Rev. Lett. **74**, 2405 (1995).

[37] Y. Aharonov and L. Vaidman, Phys. Rev. A **41**, 11 (1990).

[38] J. P. Weber and S. Wang, Opt. Lett. **15**, 526 (1990).

[39] F. Ghiringhelli, C. Alegria, and M. N. Zervas, in *Bragg Gratings, Photosensitivity, and Poling in Glass Waveguides*, OSA Technical Digest (Optical Society of America, Washington DC, 2001), paper BWA3.

[40] R. Feced and M. N. Zervas, J. Lightwave Technol. **18**, 90 (2000).

[41] S. H. Lin, K. Y. Hsu, and P. Yeh, Opt. Lett. **25**, 1582 (2000).